^{13}C pNMR of "Crumple Zone" Cu(II) Isophthalate Metal-Organic Frameworks

Daniel M. Dawson*, Charlotte E. F. Sansome, Lauren N. McHugh, Matthew J. McPherson, Laura J. McCormick McPherson, Russell E. Morris and Sharon E. Ashbrook*

Supporting Information

S1. Further NMR Experimental Details

S2. Positions of the C1 Resonances for STAM-1 and the STAM-17 Series

S3. Details of Relaxation Measurements

S4. Additional NMR Data for STAM-17-OR (R = Et, ^{n}Pr, ^{n}Bu, ^{i}Bu)

S5. References

S1. Further NMR Experimental Details

For magic angle spinning (MAS) spectra, samples were packed into zirconia rotors with an outer diameter of 1.9 mm and rotated at rates of up to 40 kHz (9.4T) or zirconia rotors with an outer diameter of 1.3 mm and rotated at rates of up to 60 kHz (14.1 T). Spectra were recorded using a rotor-synchronised spin-echo sequence, with an echo interval of one rotor period (between 16.7 and 26.7 μs). The radiofrequency field strength for all experiments was ν_1 = 125 kHz. The longitudinal relaxation constants, T_1, were measured using inversion recovery experiments and analysed using the Dynamics Centre in TopSpin versions 3.5.6 or 4.0.6 (Bruker). In all cases, the sample temperature was controlled using a Bruker BCU-II chiller and BVT/BVTB 3000 temperature controller and heater booster. Further details are given in Table S1.1.

Table S1.1. Experimental parameters: external field strength (B_0), MAS rate (ν_R), number of transients, recycle interval, for the experiments reported.

Material	experiment	B_0 / T	ν_R / kHz	transients	recycle interval / ms
STAM-1	spin echo	14.1	60.0	327680	20
	VT spin echo	9.4	37.5	32768	100
	inv. rec.[a]	9.4	37.5	8192	100
STAM-17-Me	VT spin echo	9.4	37.5	16384	100
	spin echo	14.1	55	945152	50
	inv. rec.[a]	9.4	37.5	3200	1000
STAM-17-OMe	VT spin echo	9.4	37.5	24576	100
	spin echo	14.1	55.0	1493232	50
	inv. rec.[a]	9.4	37.5	2720	1000
STAM-17-OEt	VT spin echo	9.4	37.5	14336	100
	spin echo	14.1	55.0	932960	50
	inv. rec.[a]	9.4	37.5	3328	1000
	T_2' echo	9.4	37.5	10240	200
STAM-17-O^{n}Pr	VT spin echo	9.4	37.5	65536	100
	spin echo	14.1	50.0	884736	50
	inv. rec.[a]	9.4	37.5	3152	1000
STAM-17-O^{n}Bu	VT spin echo	9.4	37.5	12288	100
	spin echo	14.1	55.0	890880	50
	inv. rec.[a]	9.4	37.5	3808	1000
as-made STAM-17-O^{i}Bu	spin echo	9.4	37.5	65536	100
rehydrated STAM-17-O^{i}Bu	VT spin echo	9.4	37.5	49152	100
	inv. rec.[a]	9.4	37.5	3360	1000
dehydrated HKUST-1	spin echo	9.4	37.5	16384	100
dehydrated STAM-1	spin echo	9.4	40.0	163840	100
dehydrated STAM-17-OEt	spin echo	9.4	40.0	40960	100

[a]. inv. rec. = inversion recovery, used for T_1 measurements.

S2. Positions of the C1 Resonances for STAM-1 and the STAM-17 Series

Figure S2.1 shows the C1 resonances for STAM-1 and the STAM-17 series recorded at 14.1 T without temperature control (estimated temperature of ~348 K, accounting for frictional heating). The corresponding spectrum for STAM-17-O^{i}Bu was not recorded.
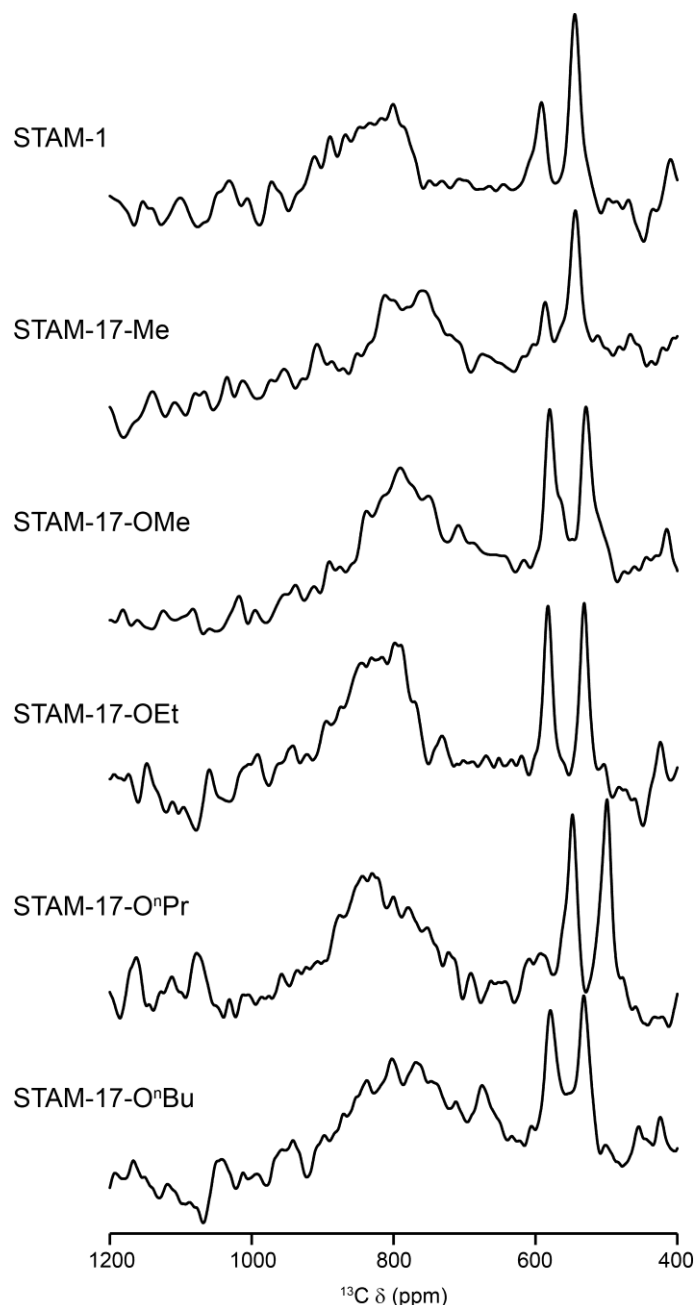
Figure S2.1. ^{13}C (14.1 T, 50-60 kHz MAS, ~348 K) NMR spectra of STAM-1 and the STAM-17 series, showing the C1 resonances. The sharper signals below 600 ppm are spinning sidebands of C3-5 (C3-6 for STAM-1). All spectra shown are processed with 2 kHz Lorentzian broadening.

S3. Details of Relaxation Measurements

All T_1 values quoted in the main text were measured by an inversion recovery experiment. Ideally, this requires a recycle interval in excess of 5 T_1 so, based on our previous observations with similar Cu(II)-based systems, an interval of 1 s was selected to allow accurate measurement of T_1 for even the slowest-relaxing C species. However, this accuracy comes at the cost of overall signal to noise ratio (compare the numbers of transients for T_1 measurements and VT spin echo experiments in Table S1.1). Another major source of error in the inversion recovery experiment is a falsely short recovery time arising from incomplete inversion – a particular concern with the large spectral widths encountered in paramagnetic systems. All values were measured at 9.4 T with a radiofrequency nutation rate ν_1 of 125 kHz for all pulses, ensuring close to ideal inversion for all resonances. T_1 values were calculated from the inversion recovery dataset using the Dynamics Centre as implemented in TopSpin versions 3.5.6 and 4.0.6.

T_2^* values (related to the observed linewidth) were estimated using DMFit,[S1] assuming that the dominant contribution to linewidth was, indeed, paramagnetically-induced T_2 relaxation rather than a chemical shift distribution. For resonances corresponding to the linker side groups, this may, in some cases, be a poor assumption owing to the disordered nature of the alkyl chains in the hydrophobic pores, which is reflected in the increased Gaussian contribution required to achieve a satisfactory spectral fit.

For STAM-17-OEt, T_2' (related to the refocusable linewidth - see Ref. [S2] for further details) was measured by a rotor-synchronised variable-time spin-echo experiment at 9.4 T with a radiofrequency nutation rate ν_1 of 125 kHz for all pulses, ensuring close to ideal inversion for all resonances. The integrated intensities as a function of echo delay were fitted to a mono-exponential decay using the Dynamics Centre as implemented in TopSpin 4.0.6.

S4. Additional NMR Data for STAM-17-OR (R = Et, *n*Pr, *n*Bu, *i*Bu)

STAM-17-OEt

Figure S4.1 shows the VT ^{13}C MAS NMR spectra of STAM-17-OEt and Table S4.1 shows the pNMR parameters for the material.
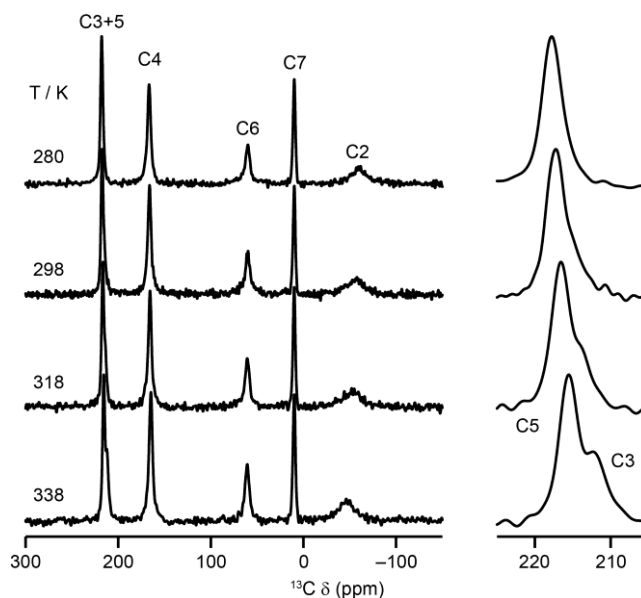

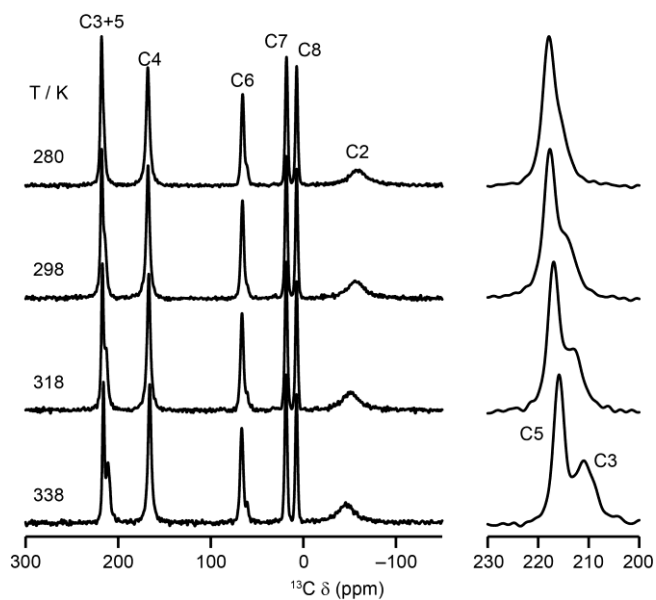**Figure S4.1**. VT ^{13}C (9.4 T, 37.5 kHz MAS) NMR spectra of STAM-17-OEt.

Table S4.1. ^{13}C pNMR parameters for STAM-17-OEt.

Assignment	δ_{iso} at 298 K (ppm)	T_1 at 298 K / ms	T_2^* at 298 K / ms	T_2' at 298 K / ms
C2	–56.1	1.40	0.18	0.12
C3	214.7	9.15[a]	0.84	1.35
C4	166.3	8.16	0.74	1.08
C5	217.4	9.15[a]	1.1	2.30
C6	60.2	19.0	0.52	1.30
C7	10.0	28.9	1.1	3.96

[a]. These resonances are overlapped under the experimental conditions used for T_1 measurement and only one combined value was determined for both species.

For STAM-17-OEt, the values of T_2^* and T_2' were compared by measuring T_2' as described above (see values in Table S4.1). It can be seen that, as would be expected, T_2' is greater than T_2^* for all species except C2, for which the difference between the two reported values is likely within the experimental error. With a rotor period, τ_r of 26.67 µs, signal for C2 was only observed for the first five data points (τ_{total} = 2, 4, 6, 8, 10 τ_r), leading to a significantly greater error in measuring T_2^* and T_2' for this species. For all other sites, signal was observed for at least 18 data points, allowing a more precise value of T_2' to be measured. T_2^* is much smaller than T_2' for the side chain C6 and C7, which, as mentioned above, would be expected if these species were more disordered, leading to a chemical shift distribution that will contribute to a reduction in T_2^* but will have no effect on T_2'.

Figure S4.2 shows the VT ^{13}C MAS NMR spectra of STAM-17-O^{n}Pr and Table S4.2 shows the pNMR parameters for the material.

Figure S4.2. VT ^{13}C (9.4 T, 37.5 kHz MAS) NMR spectra of STAM-17-O^{n}Pr.

Table 4.2. ^{13}C pNMR parameters for STAM-17-O^{n}Pr.

Assignment	δ_{iso} at 298 K (ppm)	T_1 at 298 K / ms	T_2^* at 298 K / ms
C2	−56.7	1.93	0.15
C3	214.2	6.75	0.79
C4	167.8	8.27	0.75
C5	217.7	13.0	1.2
C6	65.8	15.6	0.76
C7	18.5	24.1	0.90
C8	7.3	36.6	0.94

STAM-17-O^{n}Bu

Figure S4.3 shows the VT ^{13}C MAS NMR spectra of STAM-17-O^{n}Bu and Table S4.3 shows the pNMR parameters for the material.
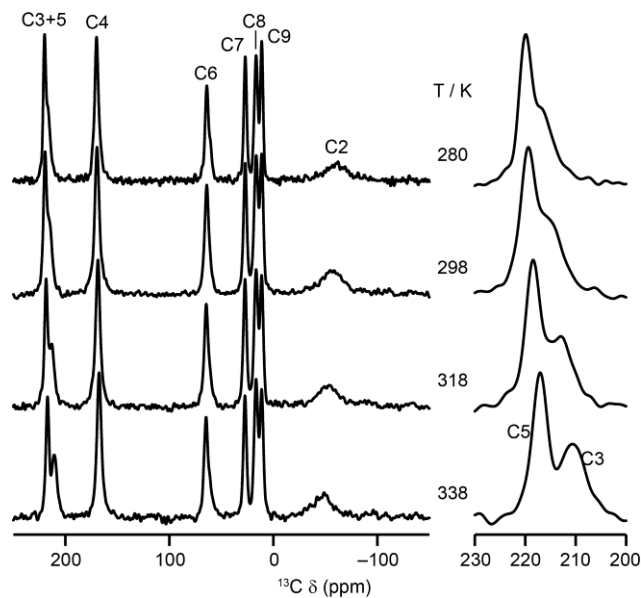

**Figure 4.3**. VT ^{13}C (9.4 T, 37.5 kHz MAS) NMR spectra of STAM-17-O^{n}Bu.

Table 4.3. ^{13}C pNMR parameters for STAM-17-O^{n}Bu.

Assignment	δ_{iso} at 298 K (ppm)	T_1 at 298 K / ms	T_2^* at 298 K / ms
C2	–56.5	1.29	0.12
C3	215.0	6.14	0.42
C4	169.5	8.41	0.73
C5	219.5	13.5	1.3
C6	64.0	14.7	0.75
C7	27.1	24.9	1.0
C8	16.6	28.0	0.80
C9	11.3	35.9	1.0

STAM-17-OⁱBu

The ^{13}C MAS NMR spectrum of as-prepared STAM-17-O^{i}Bu (Figure S4.4) contains eight resonances between 300 and –150 ppm, at 219.7, 213.8, 169.6, 71.2, 60.3, 23.9, 16.8 and –56.8 ppm. This is more than the seven expected from the structure of the linker and there are two resonances in the alkoxy region (71.2 and 60.3 ppm), whereas only one such species is be expected. Upon activation and subsequent rehydration by exposure to ambient moisture, the resonance at 60.3 ppm disappears, confirming its assignment as residual ethanol from the synthesis (the resonance from the ethanolic CH_3 is masked by the intense resonances from the MOF at 23.9 and 16.8 ppm). As shown in Figure S4.5, the ^{13}C MAS NMR spectrum of rehydrated STAM-17-O^{i}Bu contains seven resonances between 300 and –150 ppm. Table S4.4 shows the pNMR parameters for the resonances in STAM-17-O^{i}Bu.
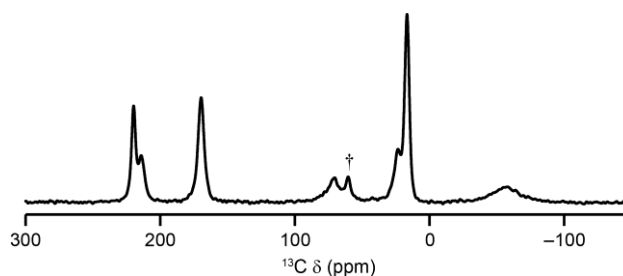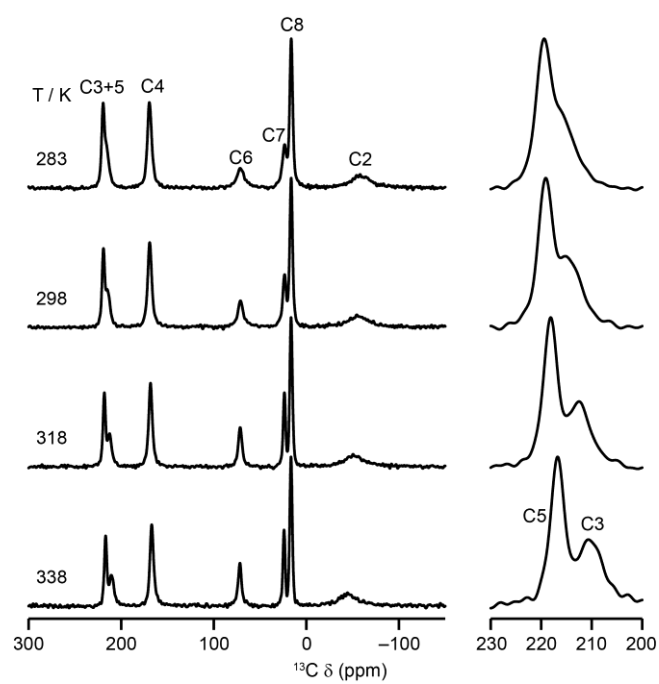

Figure S4.4. ^{13}C (9.4 T, 37.5 kHz MAS, 298 K) NMR spectrum of as-made STAM-17-O^{i}Bu. The resonance arising from ethanol is denoted with a dagger (†).

Table S4.4. ^{13}C pNMR parameters for rehydrated STAM-17-O^{i}Bu.

Assignment	δ_{iso} at 298 K (ppm)	T_1 at 298 K / ms	T_2^* at 298 K / ms
C2	–56.1	1.59	0.10
C3	214.3	9.85[a]	0.60
C4	169.1	9.13	0.66
C5	219.1	9.85[a]	0.99
C6	71.1	16.8	0.43
C7	23.8	29.4	0.87
C8	16.4	32.6	0.99

[a]. These resonances are overlapped under the experimental conditions used for T_1 measurement and only one combined value was determined for both species.

Figure S4.5. VT ^{13}C (9.4 T, 37.5 kHz MAS) NMR spectra of rehydrated STAM-17-O^{i}Bu.

S5. References

[S1] D. Massiot, F. Fayon, M. Capron, I. King, S. Le Calvé, B. Alonso, J.-O. Durand, B. Bujoli, Z. Gan, G. Hoatson, Modelling One- and Two-Dimensional Solid-State NMR Spectra. Magn. Reson. Chem. 40 (2002) 70–76. DOI: 10.1002/mrc.984.

[S2] B. Elena, A. Lesage, S. Steuernagel, A. Böckmann, L. Emsley, Proton to Carbon-13 INEPT in Solid-State NMR Spectroscopy. J. Am. Chem. Soc. 127 (2005) 17296–17302. DOI: 10.1021/ja054411x